

Spectroscopic Properties, Conformation and Structure of Difluorothiophosphoryl Isocyanate in the Gaseous and Solid Phase

Jan Schwabedissen,^[a] Pia C. Trapp,^[a] Hans-Georg Stammer,^[a] Norbert W. Mitzel,^{*[a]} Zhuang Wu,^[b] Xianxu Chu,^[b] and Xiaoqing Zeng^{*[b]}

Difluorothiophosphoryl isocyanate, $F_2P(S)NCO$ was characterized with UV/vis, NMR, IR (gas and Ar-matrix), and Raman (liquid) spectroscopy. Its molecular structure was also established by means of gas electron diffraction (GED) and single crystal X-ray diffraction (XRD) in the gas phase and solid state, respectively. The analysis of the spectroscopic data and molecular structures is complemented by extensive quantum-chemical calculations. Theoretically, the C_s symmetric *syn*-conformer is predicted to be the most stable conformation. Rotation about the P–N bond requires about 9 kJ mol^{-1} and the

predicted existence of an *anti*-conformer is dependent on the quantum-chemical method used. This *syn*-orientation of the isocyanate group is the only one found in the gas phase and contained likewise in the crystal. The overall molecular structure is very similar in gas and solid, despite in the solid state the molecules arrange through intramolecular O...F contacts into layers, which are further interconnected by S...N, S...C and C...F contacts. Additionally, the photodecomposition of $F_2P(S)NCO$ to form CO, $F_2P(S)N$, and F_2PNCO is observed in the solid Ar-matrix.

1. Introduction

Covalent isocyanates, XNCO, are frequently used building blocks in synthetic and materials chemistry.^[1] Prominent industrially-used examples are toluene diisocyanates and methylene diphenyl isocyanate, which are utilized for rigid and flexible polyurethane products as thermoplastic elastomers and thermoset resins.^[2] These isocyanates easily undergo self-addition reactions in the form of dimers and trimers yielding uretdiones or isocyanurates, respectively. Isocyanates bonded to main-group elements are of particular interest regarding their spectroscopic, conformational and structural properties. In recent years the synthesis and characterization of boryl isocyanates, R_2BNCO ,^[3] silyl isocyanates, R_3SiNCO ,^[4] alkyl isocyanates, $(R)NCO$,^[5] sulphenyl isocyanates, $RSNCO$,^[6] acyl isocyanates, $RC(O)NCO$ ^[7] and sulphonyl isocyanates, $RS(O)_2NCO$ ^[8] have

been explored by experiment and theory. The latter two, namely the acyl and sulphonyl isocyanates, exhibit significantly different structural and spectroscopic properties than the respective alkyl or sulphenyl compounds with the atom bearing the isocyanate group in a lower oxidation state.

The intrinsic structural and conformational properties of phosphorus-bonded isocyanates are of special interest, because phosphorylated urethanes and ureas are used as flame-retarding materials.^[9] Furthermore, some α -oxo-isocyanates like phosphoryl isocyanates, $R_2P(O)NCO$, show physiological activity and find applications in insecticides and drugs.^[10]


Dichlorophosphanyl isocyanate (Cl_2PNCO) ^[11] and dichlorophosphoryl isocyanate $[Cl_2P(O)NCO]$ ^[12] is the only complementary pair of phosphorus(III) and phosphorus(V) compounds bearing isocyanate groups that has been characterized so far, spectroscopically and structurally, both in the solid state as well as in the gas phase. Quantum-chemical calculations predict *syn*- and *anti*-conformations for both phosphorus compounds in the different oxidation states with barriers to interconversion lower than 3 kJ mol^{-1} . In the *syn*-conformer the NCO group is oriented to the same side of the P–N bond as the lone pair (lp) or the phosphoryl function for Cl_2PNCO and $Cl_2P(O)NCO$, respectively. Thus, in the *syn*-conformers the dihedral angle (lp/O)PNC is 0° and in the respective *anti*-conformers this angle is 180° . In the condensed phase, X-ray diffraction revealed aggregation of single molecules by O...C contacts. For the phosphorus(III) compound aggregation into endless chains by interactions between the isocyanate oxygen atom and a carbon atom of the neighbouring molecule is observed. However, for the respective phosphorus(V) compound dimers are found in the solid state, made up by contacts of the phosphoryl oxygen atom to the isocyanate carbon atom of a neighbouring molecule.


[a] Dr. J. Schwabedissen, P. C. Trapp, Dr. H.-G. Stammer, Prof. Dr. N. W. Mitzel
Fakultät für Chemie, Lehrstuhl für Anorganische Chemie und Strukturchemie
Universität Bielefeld

Universitätsstraße 25
33615 Bielefeld (Germany)
E-mail: mitzel@uni-bielefeld.de

[b] Z. Wu, X. Chu, Prof. Dr. X. Zeng

College of Chemistry
Chemical Engineering and Materials Science
Soochow University
Suzhou 215123 (China)
E-mail: xqzeng@suda.edu.cn

 Supporting information for this article is available on the WWW under <https://doi.org/10.1002/open.202000167>

 © 2020 The Authors. Published by Wiley-VCH GmbH. This is an open access article under the terms of the Creative Commons Attribution Non-Commercial License, which permits use, distribution and reproduction in any medium, provided the original work is properly cited and is not used for commercial purposes.

In the gas phase, however, different behaviours were observed, namely dynamic ones. The isocyanate group of the phosphorus(III) compound Cl_2PNCO exhibits a fully dynamic character, i.e. the NCO moiety adopts all orientations about the P–N bond relative to the lone pair at phosphorus, which were weighted and taken into account in the refinement of the GED diffraction pattern. In contrast, the gas-phase structure of the phosphorus(V) compound $\text{Cl}_2\text{P}(\text{O})\text{NCO}$ could be refined with a local dynamic model, i.e. small but significant deviations of the orientation of the isocyanate group for the *syn*- and *anti*-conformation were taken into account.

The corresponding fluorinated pair F_2PNCO ^[13] and $\text{F}_2\text{P}(\text{O})\text{NCO}$ ^[14] have been investigated as well. Quantum-chemical calculations proposed the existence of *syn*- and *anti*-conformers for both compounds.^[15] Anyhow, the fluorinated phosphorus(III) compound F_2PNCO was examined solely by gas-phase electron diffraction revealing the exclusive presence of a *syn*-conformer. And the phosphoryl compound was examined only by X-ray diffraction of single crystals, which reveal a dimer formation comparable to the aggregation motive of $\text{Cl}_2\text{P}(\text{O})\text{NCO}$.

In this contribution we describe the structural properties and thus the influence of the sulphur atom of difluorothiophosphoryl isocyanate, $\text{F}_2\text{P}(\text{S})\text{NCO}$, in the solid state and in the gas phase. The investigation is complemented by the elucidation of the vibrational properties (IR and Raman) and its photo-decomposition in an Ar-matrix.

2. Results and Discussion

2.1. Quantum Chemical Calculations

In order to locate the possible conformers of $\text{F}_2\text{P}(\text{S})\text{NCO}$ on the potential hypersurface, several energy profiles for the rotation of the isocyanate group around the P–N bond were calculated. The results of the energy curves are shown in Figure 1.

The potentials were calculated at the different levels of theory and all predict the *syn*-conformer to be the most stable. In the *syn*-conformation, the isocyanate group is located

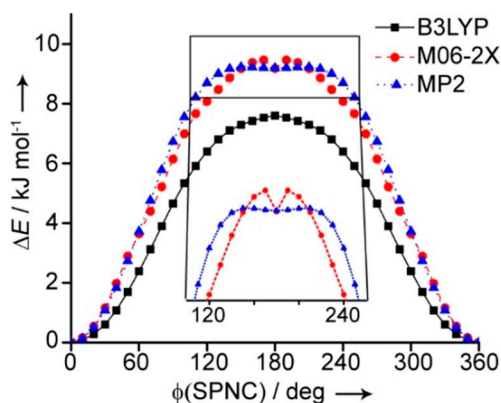


Figure 1. Potential energy scan for the rotation of the isocyanate group around the P–N bond based on different methods all using the cc-pVTZ basis set. The upper marked box is provided stretched in the energy-dimension in the box below.

coplanar to the thiophosphoryl moiety. However, the calculations using the MP2^[26] *ab initio* method and the M06-2X^[27] density functional theory predict a shallow minimum with a dihedral angle $\varphi(\text{SP-NC})$ of 180° (*anti*). Both possible conformers are depicted in Figure 2. The barrier for the interconversion calculated on the basis of the two mentioned methods is approximately 1.5 kJ mol^{-1} higher than the respective one for the B3LYP^[28] calculation, which is 7.5 kJ mol^{-1} .

The potential energy scan of the oxide $\text{F}_2\text{P}(\text{O})\text{NCO}$ ^[14] features the same behaviour with a flat minimum about the *anti*-conformation with the interconversion barrier being about 2 kJ mol^{-1} lower than in the case examined here. The analogous phosphorus(III) species F_2PNCO shows only one stable conformer as well.^[13,15] Dichlorophosphoryl isocyanate shows two stable conformers, *syn* and *anti*, and the barrier to rotation amounts to $2\text{--}3 \text{ kJ mol}^{-1}$ depending on the method and basis set employed for its calculation.^[12] Furthermore, different basis set/method combinations predict different energetically preferred conformers for dichlorophosphanyl isocyanate.^[11] Thus, the high barrier for rotation and the strong preference of the *syn*-conformer in $\text{F}_2\text{P}(\text{S})\text{NCO}$ is due to the substitution of the phosphorus atom with both sulphur and fluorine.

2.2. Vibrational Spectra of $\text{F}_2\text{P}(\text{S})\text{NCO}$

The IR (gas and Ar-matrix) and Raman (liquid) spectra of $\text{F}_2\text{P}(\text{S})\text{NCO}$ are shown in Figure 3. The strongest IR bands in the IR spectra (gas: 2297 cm^{-1} ; Ar-matrix: 2293 cm^{-1} , Table 1) correspond to most characteristic asymmetric NCO stretching mode ($\nu_{\text{asym}}(\text{NCO})$). They are slightly lower in frequency than those in $\text{F}_2\text{P}(\text{O})\text{NCO}$ (gas: 2309 cm^{-1} ; Ar-matrix: 2307 cm^{-1})^[14] but close to those in $\text{Cl}_2\text{P}(\text{O})\text{NCO}$ (gas: 2290 cm^{-1} ; Ne-matrix: 2289 cm^{-1}).^[12] In the Raman spectrum, it appears as a very weak band at 2286 cm^{-1} . The symmetric NCO stretching mode ($\nu_{\text{sym}}(\text{NCO})$) occurs at 1439 and 1428 cm^{-1} in IR (Ar-matrix) and Raman (liquid) spectra, respectively. The shift in the band positions indicates weak interactions involving the NCO moiety in the condensed phase. The two PF_2 stretching modes, $\nu_{\text{sym}}(\text{PF}_2)$ and $\nu_{\text{asym}}(\text{PF}_2)$, located at 950 and 927 cm^{-1} in the IR spectrum of gaseous $\text{F}_2\text{P}(\text{S})\text{NCO}$ as a broad band; they are quite close to the two well-resolved bands in the Ar-matrix at 947 and 919 cm^{-1} . In the Raman spectrum, only two very weak bands at 940 and 911 cm^{-1} were observed. Interestingly, a weaker band at 793 cm^{-1} appears beside the IR band at

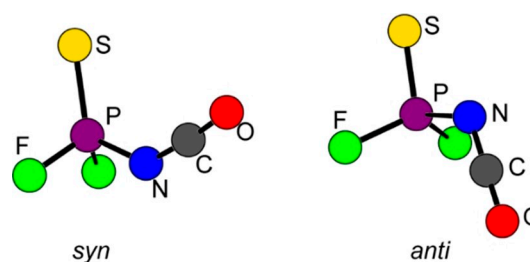


Figure 2. Optimized minimum structures of difluorothiophosphoryl isocyanate (1).

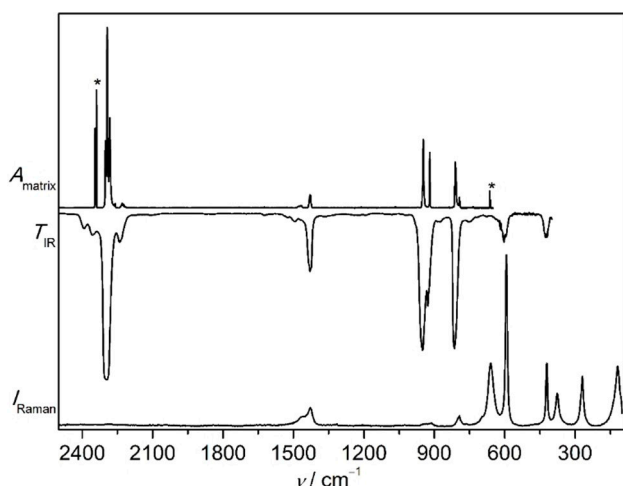


Figure 3. Upper trace: IR spectrum of $F_2P(S)NCO$ isolated in an Ar-matrix at 2.8 K (absorbance A , resolution: 0.5 cm^{-1}). Middle trace: IR spectrum of gaseous $F_2P(S)NCO$ at 300 K (transmission T , resolution: 2 cm^{-1}). Lower trace: Raman spectrum of liquid $F_2P(S)NCO$ at 300 K (Raman intensity I , resolution: 2 cm^{-1}). Bands associated with CO_2 are marked with asterisks.

Table 1. Experimentally observed and calculated vibrational frequencies ($> 400\text{ cm}^{-1}$) of $F_2P(S)NCO$.

observed ^[a] IR (gas)	IR (matrix)	Raman (liquid)	Calculated (I_{IR}) [I_{Raman}] ^[b]	Assignment ^[c]
2297 vs	2293.4 vs	2286 vw	2372 (1434) [5]	$\nu_{asym}(NCO)$
1430 m	1439.2 m	1428 m	1486 (105) [22]	$\nu_{sym}(NCO)$
950 s	946.5 s	940 vw	924 (338) [1]	$\nu_{sym}(PF_2)$
927 s	919.3 s	911 w	891 (142) [2]	$\nu_{asym}(PF_2)$
814 s	810.3 s	793 m	785 (312) [5]	$\nu(PN)$
677 vw	663.5 m	659 s	656 (8) [7]	$\nu(PS)$
603 w			619 (24) [< 1]	$\delta_{a.p.}(NCO)$
596 w		591 vs	589 (23) [22]	$\delta_{i.p.}(NCO)$
425 w		419 s	411 (21) [2]	$\delta(PF_2)$

[a] Band positions and intensities: vs very strong, s strong, m medium strong, w weak, vw very weak. [b] Calculated harmonic IR frequencies at the B3LYP/6-311+G(3df) level of theory, IR intensities (km mol^{-1}) in parentheses and Raman intensities ($\text{\AA}^4\text{ amu}^{-1}$) in square brackets. [c] Tentative assignment based on the calculated vibrational displacement vectors of $F_2P(S)NCO$.

811 cm^{-1} for the P–N stretching mode, whereas, only one band at 814 cm^{-1} is present in the gas-phase IR spectrum. This side band is more likely due to the matrix-site effect rather than the presence of a second conformer, since the relative intensity of the two IR bands remains almost unchanged when the vacuum deposition of $< F_2P(S)NCO/Ar$ was accompanied with heating to ca. 200°C . The band position (810 cm^{-1}) is significantly higher than the P–N stretching modes in $F_2P(O)NCO$ (751.8 cm^{-1} , Ar-matrix)^[14] and $Cl_2P(O)NCO$ (747 cm^{-1} , Ne-matrix).^[12] The P=S stretching mode in $F_2P(S)NCO$ (659 cm^{-1} , Raman) is reasonably lower than those in F_3PS (696 cm^{-1} , Raman)^[29] due to lower electronegativity of pseudohalogen NCO than F.

2.3. Photodecomposition of $F_2P(S)NCO$

Given the frequently observed photolytic CO-elimination in covalent isocyanates $R-NCO$ ($\rightarrow RN + CO$, $R=OCN(O)-$,^[30] $MeOC(O)-$,^[31] $Me_2NC(O)-$ ^[32]), the photochemistry of $F_2P(S)NCO$ in solid Ar-matrix was also studied. Upon an ArF excimer laser (193 nm) irradiation, decomposition of $F_2P(S)NCO$ occurs as evidenced by the depletion of its IR band (Figure 4, lower trace). As a result, the IR bands for CO (e, 2140.2 cm^{-1}),^[33] $F_2P(S)N$ (b, 1184.2 , 927.1 and 872.4 cm^{-1}) and F_2PNS (c, 1223.2 , 841.2 and 823.9 cm^{-1})^[34] appear. Additionally, a new species displaying a distinguishable IR band at 2271.7 cm^{-1} (f) also forms, and it coincides with the strongest IR band for F_2PNCO (2271 cm^{-1} , Ar-matrix).^[35] Therefore, sulphur-elimination in $F_2P(S)NCO$ also happens under laser irradiation at 193 nm , whereas, no IR band for further CO-elimination product (F_2PN) could be identified among the photolysis products. The assignment for the IR band at 2201.3 cm^{-1} (labelled with an asterisk in Figure 3) remains unclear.

Subsequent irradiation of the Ar-matrix with UV-light (365 nm) mainly results in the transformation of F_2PNS (c) to F_2PSN (d, 1177.0 , 846.0 and 814.1 cm^{-1}). Traces of $F_2P(S)NCO$ (a) reforms by recombining the singlet thiophosphoryl nitrene $F_2P(S)N$ with CO in same matrix cages. Similar photolytic CO-association reactions have been previously observed for the phosphorus analogue of nitrous oxide ($OPN + CO \rightarrow OPNCO$)^[36] and phenylborylene ($PhB + CO \rightarrow PhBCO$)^[37]

2.4. Gas-Phase Structure

The structure of free molecules of $F_2P(S)NCO$ was determined by gas-phase electron diffraction. The refinement of the gas-phase structure was performed using a one-conformer model based on the *syn*-conformer as suggested by quantum-chemical

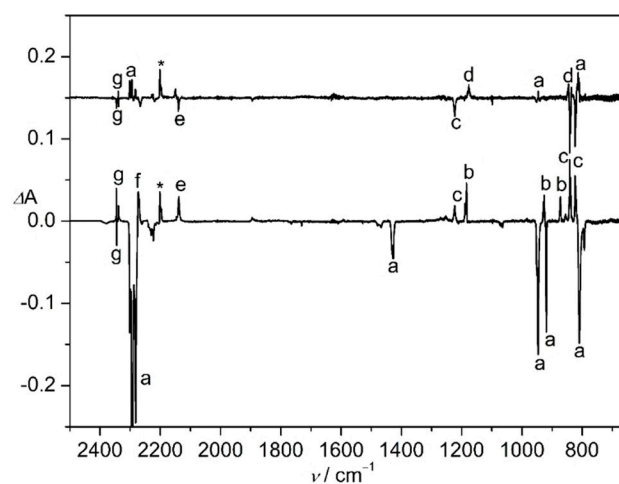


Figure 4. Lower trace: IR difference spectrum reflecting the change of Ar-matrix isolated $F_2P(S)NCO$ upon an ArF laser photolysis (3 Hz, 3 mJ, 25 min). Upper trace: IR difference spectrum reflecting the change of the matrix upon subsequent 365 nm light irradiation (48 W, 30 min). The IR bands of $F_2P(S)NCO$ (a), $F_2P(S)N$ (b), F_2PNS (c), F_2PSN (d), CO (e), F_2PNCO (f), CO_2 (g) and an unknown species (*) are labelled.

calculations. The refined model resulted in overall a disagreement factor R_f of 2.6%. The radial distribution curve is depicted in Figure 5 also containing some labelled interatomic distances of the *syn*-conformer. Table 2 compares the structural parameters of the gas-phase electron diffraction refinement of difluorothiophosphoryl isocyanate with the other phosphorus-bonded isocyanates and azides. In the series of the investigated phosphorus-bonded pseudohalides $F_2P(S)NCO$ is one of the two compounds whose gas-phase structures were determined using a one-conformer model. The other one is the related phosphorus(III) species F_2PNCO .^[13] The isocyanate group in all cases is almost linear, i.e. $\angle(NCO)$ is always larger than 170° , and the bond lengths in this unit do not vary much in the examples listed in Table 2.^[38] Comparing the P–S bond length to the analogous distances in $PF_2H(S)$, $PClF_2(S)$ and $PBrF_2(S)$ (the reported r_a values (1.876(3), 1.864(8) and 1.881(4) Å, respectively)^[39] the one determined for $F_2P(S)NCO$ (1.874(1) Å) is most similar to the length found for the hydrogen compound $PF_2H(S)$. The P–N bond length of $F_2P(S)NCO$ is also the shortest among the examples listed in Table 2. This confirms the effect

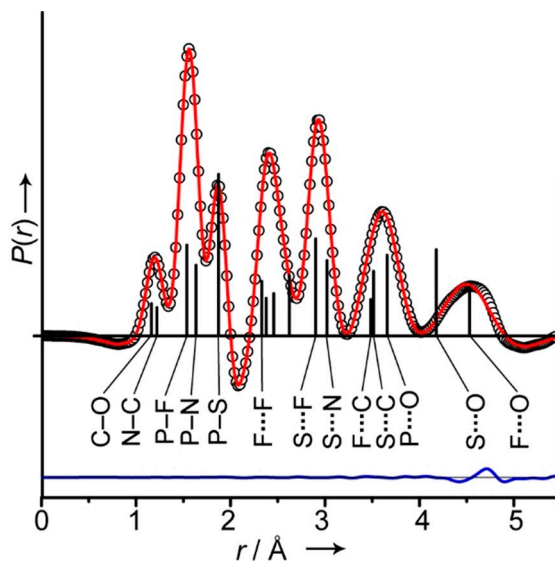


Figure 5. Experimental (circles \circ) and model (continuous line $-$) radial distribution functions of $F_2P(S)NCO$ (1). The difference curve is shown below. Vertical bars indicate interatomic distances of the *syn*-conformer; selected ones are labelled.

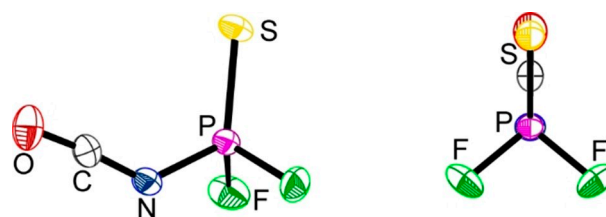


Figure 6. Molecular structure in the solid state of $F_2P(S)NCO$. Right: view along the P–N bond confirming the C_2v symmetry. The symmetry operation for generating equivalent positions is $(+x, -y, +z)$ for (').

of strongly electron-withdrawing substituents^[40] and the heavy-atom effect^[41] in shortening bond length due to lowering the anti-bonding orbitals which is then more available for conjugation. The bond lengths of the isocyanate group are in good accordance to the previously determined parameters of the phosphorus bonded isocyanates.

2.5. Solid-State Structure

The technique of *in situ* crystallisation was applied to obtain a single crystal of $F_2P(S)NCO$ as the substance is a liquid at ambient conditions. Details of the procedure as well as crystallographic details are provided in the experimental section (Table 4). Figure 6 shows the molecular structure. Relative to the gas-phase structure no significant variations of the geometrical parameters are observed for the solid-state structure.

In the crystal structure the isocyanate $F_2P(S)NCO$ molecule lies on a crystallographic mirror plane of symmetry with its thiophosphoryl moiety and the isocyanate group; it thus has C_s symmetry. In the row of the previously investigated solid-state structures of phosphorus pseudo halides, the thiophosphoryl isocyanate is the first example, which lies on a crystallographic mirror plane. This confirms the conformational stability of $F_2P(S)NCO$ predicted theoretically and observed experimentally in the gas phase. The structure of $F_2P(O)N_3$ in the solid state occupies C_s symmetry within the error range.^[14] Concerning the geometrical parameters of the isocyanate group the N–C and C–O lengths are the same within error limits for the isocyanates bound to a phosphorus atom in the formal oxidation state +V. However, in the phosphorus(III) isocyanate Cl_2PNCO ^[11] the N–C

Table 2. Structural parameters of the gas-phase structure of $F_2P(S)NCO$ and related molecules.

	reference	$r(P=X)$	$r(PN)$	$r(N=C)$	$r(C=O)$	$r(P-Y)$	$\angle(XPN)$	$\angle(PNC)^{[b]}$	$\angle(NCO)^{[b]}$	$\angle(Y-P-Y)$
$F_2P(S)NCO$, $r_g^{[c]}$	this work	1.874(1)	1.635(1)	1.223(1)	1.164(1)	1.539(1)	119.2(3)	136.0(4)	174.0(4)	98.3(2)
$Cl_2P(O)NCO$, $r_g^{[c]}$	12	1.442(1)	1.646(1)	1.212(1)	1.157(1)	1.995(1)	118.3(2)	135.8(2)	175.3(2)	102.8(1)
Cl_2PNCO , $r_g^{[c]}$	11		1.667(3)	1.203(1)	1.159(1)	2.045(1)		137.2(6)	171.5(6)	99.4(2)
$F_2P(O)N_3$, $r_{h1}^{[d]}$	14	1.437(4)	1.657(2)	1.251(3)	1.130(2)	1.531(6)	118.9(3)	117.8(5)	172(2)	98.8(3)
F_2PN_3 , $r_{h1}^{[d]}$	15		1.716(3)	1.247(3)	1.127(3)	1.572(2)		117.7(5)	177(1)	96.4(2)
F_2PNCO , $r_a^{[e]}$	13		1.683(6)	1.256(6)	1.168(5)	1.563(3)		130.6(8)		97.9(8)

[a] Distances r in Å, angles and dihedral angles in deg. [b] For the azides the analogous parameters are given. X is the chalcogen atom and Y is the halide bonded to phosphorus. [c] r_g is the thermally averaged internuclear distance $\langle r \rangle$. [d] r_{h1} is the distance between average nuclear positions and derived from r_a : $r_{h1} = r_a + u^2/r_a - r_{anh} - \Delta r_{anh} - \delta r$, with r_a see [e], r_{anh} is a correction for anharmonic vibration, δr is a small correction due to centrifugal distortion and u being the vibrational amplitude. [e] r_a is the internuclear distance directly accessible by GED $\langle 1/r \rangle^{-1}$, $r_a = r_g - u^2/r_e$ ($\cong r_g - u^2/r_e$) with u being the vibrational amplitude and r_e being the equilibrium distance.

Table 3. Structural parameters ^[a] of F₂P(S)NCO and related molecules in the solid state. X is the chalcogen atom and Y stands for the halide bonded to phosphorus.

	ref.	r(P=X)	r(P–N)	r(N=C) ^[b]	r(C=O) ^[b]	r(P–Y)	∠(XPN)	∠(PNC) ∠(PNN)	∠(NCO)/ ∠(NNN)	∠(Y–P–Y)	φ(OP–NC)/ φ(OP–NN)
F ₂ P(S)NCO	this work	1.881(1)	1.627(1)	1.213(1)	1.149(1)	1.533(1)	120.6(1)	132.1(1)	174.8(1)	98.8(1)	0
Cl ₂ P(O)NCO	12	1.455(1)	1.623(1)	1.213(2)	1.149(2)	1.987(1) / 1.985(1)	118.4(1)	135.2(1)	174.1(1)	103.6(1)	–38.1(1)
Cl ₂ PNCO	11		1.688(2)	1.202(2)	1.160(2)	2.054(1) / 2.049(1)		136.1(2)	174.6(2)	99.9(1)	
F ₂ P(O)NCO	14	1.438(2)	1.615(2)	1.216(3)	1.146(3)	1.519(2) / 1.517(2)	119.9(1)	132.5(2)	174.2(3)	99.4(1)	–18.9(5)
F ₂ P(O)N ₃ ^[b]	15	1.442(2)	1.639(2)	1.225(3)	1.113(3)	1.525(2) / 1.527(2)	120.1(1)	117.3(2)	173.4(3)	98.6(1)	–0.2(3)
F ₂ P(O)N ₃ ^[b]	13	1.447(2)	1.638(2)	1.247(3)	1.117(3)	1.523(2) / 1.526(2)	120.1(1)	118.6(2)	172.4(3)	99.0(1)	–0.7(3)

[a] Distances *r* in Å, angles and dihedral angles in deg. [b] In this case two crystallographically independent molecules were found.

bond is shorter and the C–O bond is longer in the solid state. The approximate linearity of the isocyanate group is also observed for the isocyanates listed in Table 3 with the angle ∠(NCO) being about 174° in all mentioned cases.

The most pronounced difference between the solid-state structure of the sample investigated here and the other isocyanates are the observed O...F contacts (Figure 7). While in the other solid-state structures interactions between either the phosphoryl or the isocyanate oxygen atom with the most electropositive carbon atom are observed, the thiophosphoryl isocyanate shows O...F contacts at 2.924(1) Å (sum of van der Waals radii: 2.96 Å).^[42] The short contact and the resulting normalized contact value^[43] of 0.98 give rise to the halogen bonding^[44] motif at the fluorine substituent with the electron donating oxygen atom. In general, halogen bonding at fluorine atoms is rarely observed except the fluorine substituent is bound to an extremely strong electron withdrawing group like the trifluoromethoxy (CF₃O–) group,^[45,46] yet it has been investigated as an amphiphilic partner in non-covalent interactions.^[47] Despite the short interatomic distance, halogen bonding is characterized by the angle at the halogen atom to be nearly 180°. In the case examined here the P–F...O angle measures 143.8(1)° and is thus far from the presumed linearity for halogen bonding. On the other hand, the C=O...F angle of 127.5(1)° suggests, assuming an approximate sp² hybridization of the oxygen atom, an interaction of the fluorine atom with the lone pair at the oxygen atom. This is affirmed by the sum of the angles at oxygen (2 × ∠(C=O...F) + ∠(F...O...F)) being 350.0(3)°

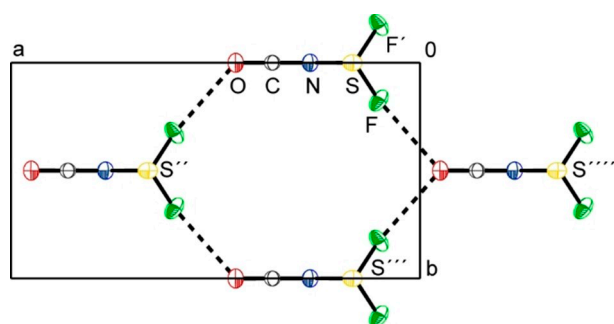


Figure 7. View on the unit cell along the crystallographic *c*-axis showing the O...F contacts. The symmetry operations for generating equivalent positions are: (+*x*, –*y*, +*z*) for ('); (½ + *x*, ½ – *y*, +*z*) for ("); (+*x*, 1 – *y*, +*z*) for ("); (–½ + *x*, ½ + *y*, +*z*) for ("").

and thus the oxygen atom is in almost planar coordination. Thus this O...F interaction can be classified as a type I interaction.^[48]

The layers built up by the mentioned O...F contacts arrange in an antiparallel manner with cancelling dipole moments. Connections to the next parallel layers are made up by S...N contacts (3.391(1) Å) shorter than the sum of the respective van der Waals radii (3.55 Å). Figure 8 depicts the arrangement of different layers.

Furthermore, the anti-parallel orientated layers are linked by S...C (3.510(1) Å) and C...F contacts (3.183(1) Å). Both distances are shorter than the sum of the van der Waals radii of the corresponding atoms, 3.66 Å for S...C and 3.23 Å for C...F.

3. Conclusion

The vibrational spectroscopy, photochemistry, conformation, and structure of difluorothiophosphoryl isocyanate, F₂P(S)NCO,

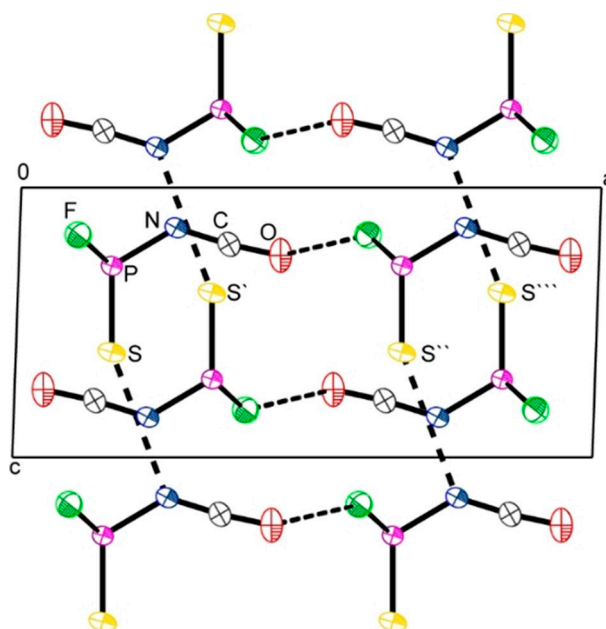


Figure 8. View along the crystallographic *b*-axis showing the assembly of parallel and anti-parallel layers in the solid-state structure of F₂P(S)NCO. The symmetry operations for generating equivalent positions are: (½ – *x*, ½ – *y*, 1 – *z*) for ('); (½ + *x*, ½ – *y*, +*z*) for ("); (+*x*, –*y*, +*z*) for ('); (1 – *x*, –*y*, 1 – *z*) for ("").

was extensively investigated by a series of techniques: UV/vis and NMR spectroscopy, IR spectroscopy in the gas and matrix, Raman spectroscopy of the liquid, gas electron diffraction and single crystal X-ray diffraction. In line with the computationally predicted preference of a *syn*-conformation in F₂P(S)NCO, the gas-phase electron diffraction finds solely the *syn*-conformer. Its structure determined in the gaseous state is very similar to the structure of the molecules embedded into a single crystal as examined by X-ray diffraction. In the solid state, the molecules arrange into layers through weak O...F contacts, and the layers are further linked by S...N, S...C and C...F contacts.

Experimental Section

Sample Preparation

Similar to the synthesis of F₂P(O)NCO,^[14] difluorothiophosphoryl isocyanate, F₂P(S)NCO was synthesized by the reaction of F₂P(S)Cl with AgNCO. Freshly distilled F₂P(S)Cl (0.14 g, 1 mmol) was condensed into a flask containing freshly dried AgNCO (0.51 g, 3 mmol) at −196 °C. The mixture was slowly warmed to room temperature and stirred for 10 h. The volatile part of the reaction mixture was then distilled by passing through three successive cold traps maintained at −70, −90 and −196 °C. Pure F₂P(S)NCO was retained in the −90 °C trap as a colourless liquid. The quality of the sample was checked using gas phase IR and ³¹P NMR spectroscopy. Vapour pressures of the liquid in the temperature range from −80 to −50 °C were recorded, from which the vaporization enthalpy (ΔH_{vap}) was determined to be 33.6 ± 0.9 kcal mol^{−1}.

IR, Raman, UV/vis, and NMR Spectroscopy

The gas-phase IR spectrum was measured in an IR gas cell (optical path length 20 cm, Si windows, 0.5 mm thickness), which was fitted into the sample compartment of the FT-IR instrument (Bruker, Tensor 27). Raman spectrum was recorded on a Bruker Equinox 55 FRA 106/S FT-Raman spectrometer using a 1064 nm Nd:YAG laser (200 mW) with 200 scans at a resolution of 2 cm^{−1}. The UV/vis spectrum of F₂P(S)NCO recorded by Shimadzu UV 3600, which exhibits strong absorption at 197 nm. ³¹P NMR spectrum was measured in CDCl₃ solution at room temperature using a Bruker Avance 400 spectrometer (242.8 MHz), a triplet at 34.5 ppm [¹J(³¹P¹⁹F) = 1311 Hz] was observed for F₂P(S)NCO.

Matrix IR Spectroscopy

Matrix IR spectra were recorded on a FT-IR spectrometer (Bruker 70 V) in a reflectance mode using a transfer optic. A KBr beam splitter and liquid-nitrogen-cooled MCT detector were used in the mid-IR region (4000–600 cm^{−1}). For each spectrum, 200 scans at a resolution of 0.5 cm^{−1} were co-added. The gaseous samples were mixed with argon gas (1:1000) in a 1 L stainless-steel storage container. Then the mixture passed through an aluminium oxide furnace (o.d. 2.0 mm, i.d. 1.0 mm), and immediately deposited (2 mmol h^{−1}) onto a Rh-plated copper block matrix support (2.8 K) in a high vacuum (~10^{−5} Pa). Photolysis was performed by using an ArF excimer laser (Gamlaser EX5/250, 3 Hz, 193 nm) and a high-power flashlight (Boyu T648, 365 nm, 48 W).

Quantum Chemical Calculations

A potential energy surface scan was performed on different levels of theory using the Dunning-type basis set^[16] by rotating the isocyanate group around the P–N bond. Subsequent optimizations of the minimum structures were performed on the respective combination of method and basis set including the calculation of vibrational frequencies to assure true minima. All calculations were performed using the GAUSSIAN09 quantum-chemical program at the version D.01.^[17]

Gas-Phase Electron Diffraction Experiment

The electron diffraction patterns were recorded on the heavily improved Balzers Eldigraph KD-G2 gas-phase electron diffractometer at Bielefeld University. Instrumental details are reported elsewhere.^[18] Experimental parameters are listed in Table 4. The electron diffraction patterns were measured on the Fuji BAS-IP MP 2025 imaging plates, which were scanned by using calibrated Fuji BAS 1800II scanner. The intensity curves (Figure 9) were obtained by applying the method described earlier.^[19] Sector function and electron wavelength were refined using carbon tetrachloride diffraction patterns,^[20] recorded in the same experiment as the substance under investigation.

Table 4. Details of the gas-phase electron diffraction experiment for F₂P(S)NCO.

Parameters	short detector distance	long detector distance
nozzle-to-plate distance, mm	250.0	500.0
accelerating voltage, kV	60	60
fast electron current, μA	1.52	1.52
electron wavelength, ^[a] Å	0.048770	0.048737
nozzle temperature, K	297	294
sample pressure, ^[b] mbar	$6.1 \cdot 10^{-6}$	$3.2 \cdot 10^{-6}$
residual gas pressure, ^[c] mbar	$2.0 \cdot 10^{-6}$	$5.1 \cdot 10^{-7}$
exposure time, s	15	10
used s range, Å ^{−1}	8.0–30.0	3.0–15.0
number of inflection points ^[d]	3	4
R_f factor, %	3.11	1.94

[a] Determined from CCl₄ diffraction patterns measured in the same experiment. [b] During the measurement. [c] Between measurements. [d] Number of inflection points on the background lines.

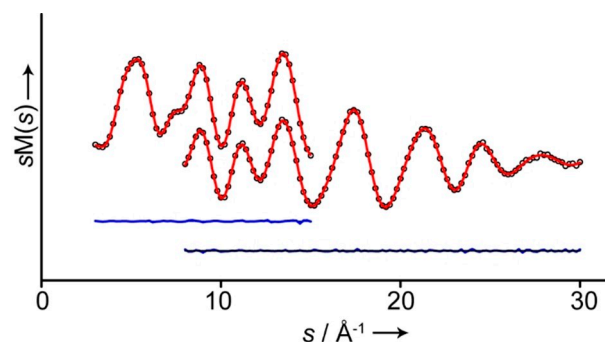


Figure 9. Experimental (○) and model (–) molecular scattering intensities and the respective differences (lower traces, experiment–model) for long (upper curves) and short (lower curves) nozzle-to-detector distances for F₂P(S)NCO (1).

Table 5. Summary of crystallographic data for F ₂ P(S)NCO.	
chemical formula	CF ₂ NOPS
<i>M_r</i>	143.05
crystal system	monoclinic
space group	C2/m (No.12)
<i>a</i> (Å)	12.6600(1)
<i>b</i> (Å)	6.6550(1)
<i>c</i> (Å)	5.8831(1)
β (°)	91.9288(9)
<i>V</i> (Å ³)	495.38(1)
<i>Z</i> / <i>Z'</i>	4 / 0.5
<i>T</i> (K)	95.0(2)
ρ_{calc} (g cm ⁻³)	1.918
μ (mm ⁻¹)	0.895
2 θ range [°]	6.44–120.15
Index range <i>h</i>	–30 to 30
Index range <i>k</i>	–16 to 15
Index range <i>l</i>	–14 to 114
Refl. collect.	130917
Indep. refl.	3941
<i>R_{int}</i>	0.0358
Data/restraints/parameters	2871/0/145
<i>R₁</i> , <i>I</i> > 2 σ (<i>I</i>) / all data	0.0296/0.0381
<i>wR₂</i> , <i>I</i> > 2 σ (<i>I</i>) / all data	0.0918/0.0975
<i>GoF</i>	1.076
$\rho_{\text{max/min}}$ [e Å ⁻³]	0.48/–0.69
CCDC	2006262

[a] *R₁* is defined as $\sum ||F_o| - |F_c|| / \sum |F_o|$ for *I* > 2 σ (*I*). [b] *wR₂* is defined as $[\sum w(F_o^2 - F_c^2)^2 / \sum w(F_o^2)^2]^{1/2}$ for *I* > 2 σ (*I*).

Gas-Phase Electron Diffraction Structural Analysis

The structural analysis was performed using the UNEX program.^[21] All refinements were performed using two averaged intensity curves simultaneously (Figure 9), one from the short and another from the long nozzle-to-detector distance. These were obtained by averaging intensity curves measured in independent experiments obtained at the same camera distance. The starting geometry for the refinement of the gas-phase structure of difluorothiophosphoryl isocyanate in *syn-conformation* was taken from the optimized structures of the M06-2X/cc-pVTZ calculations. The mean square amplitudes and vibrational corrections to the equilibrium structure were calculated with the Vibmodule program^[22] based on the M06-2X/cc-pVTZ calculations as well. Independent geometrical parameters and their groups in the least-squares refinement are listed in the Supporting Information. The bonded distances were refined in three individual groups divided based on the peaks of the radial distribution function they are located under. The angles were refined separately except the pair of \angle (PNC) and \angle (NCO) which were grouped together. During the refinement, no restraints were used and the amplitudes from the quantum-chemical calculations were not refined. Within a group, the differences were kept fixed at the computational level.

X-Ray Crystallography

A single crystal of difluorothiophosphoryl isocyanate^[23] was grown *in situ* at 181 K and cooled to 171 K at a rate of 5 K h⁻¹ and subsequently to 95 K with 200 K h⁻¹. X-Ray diffraction patterns were measured on a Rigaku Supernova diffractometer using MoK α (λ = 0.71073 Å) radiation at 95.0(2) K. Using Olex2,^[24] the structure was solved and refined with the ShelX structure solution program and refinement package.^[25] Crystal and refinement details are provided in Table 5.

Acknowledgements

This work was partially supported by the National Natural Science Foundation of China (2167314). This work was financially supported by Deutsche Forschungsgemeinschaft: core facility GED@BI (grant MI477/35-1, project no. 324757882). The authors acknowledge the funding of this project by computing time provided by the Paderborn Center for Parallel Computing (PC2) and the RRZK of Cologne University. Open access funding enabled and organized by Projekt DEAL.

Conflict of Interest

The authors declare no conflict of interest.

Keywords: difluorothiophosphoryl isocyanate · gas electron diffraction · X-ray diffraction · vibrational spectroscopy · photodecomposition

- [1] For example, see: a) S. Ozaki, *Chem. Rev.* **1972**, *72*, 457–496; b) K. Uehara, K. Fukaya, N. Mizuno, *Angew. Chem. Int. Ed.* **2012**, *51*, 7715–7718, *Angew. Chem.* **2012**, *124*, 7835–7838; *Angew. Chem. Int. Ed.* **2012**, *51*, 7715–7718; c) G. Schäfer, C. Matthey, J. W. Bode, *Angew. Chem. Int. Ed.* **2012**, *51*, 9173–9175, *Angew. Chem.* **2012**, *124*, 9307–9310.
- [2] E. Delebecq, J.-P. Pascault, B. Boutevin, F. Ganachaud, *Chem. Rev.* **2013**, *113*, 80–118.
- [3] a) A. Troiani, S. Garzoli, F. Pepi, A. Ricci, M. Rosi, C. Salvitti, G. de Petris, *Chem. Commun.* **2014**, *50*, 13900; b) R. Hausser, H. Oberhammer, W. Einholz, P. O. Paetzold, *Inorg. Chem.* **1990**, *29*, 3286.
- [4] a) G. A. Guirgis, S. M. Askarian, T. Morris, M. H. Palmer, B. H. Pate, N. A. Seifert, *J. Phys. Chem. A* **2015**, *119*, 11875; b) G. A. Guirgis, J. S. Overby, T. J. Barker, M. H. Palmer, B. H. Pate, N. A. Seifert, *J. Phys. Chem. A* **2015**, *119*, 652.
- [5] J. R. Durig, R. J. Berry, C. J. Wurrey, *J. Am. Chem. Soc.* **1988**, *110*, 718.
- [6] S. T. Vallejos, M. F. Erben, H. Willner, R. Boese, C. O. Della Védova, *J. Org. Chem.* **2007**, *72*, 9074.
- [7] a) L. A. Ramos, S. E. Ulic, R. M. Romano, Y. V. Vishnevskiy, R. J. F. Berger, N. W. Mitzel, H. Beckers, H. Willner, S. Tong, M. Ge, C. O. Della Védova, *J. Phys. Chem. A* **2012**, *116*, 11586; b) M. F. Erben, J. M. Padró, H. Willner, C. O. Della Védova, *J. Phys. Chem. A* **2009**, *113*, 13029; c) T. M. Klapötke, B. Krumm, S. Rest, R. Scharf, J. Schwabedissen, H.-G. Stämmler, N. W. Mitzel, *J. Phys. Chem. A* **2016**, *120*, 4534.
- [8] a) A. M. Betancourt, Y. B. Bava, Y. B. Martínez, M. F. Erben, R. L. C. Filho, C. O. Della Védova, R. M. Romano, *J. Phys. Chem. A* **2015**, *119*, 8021; b) A. M. Betancourt, A. F. Antognini, M. F. Erben, R. Cavasso-Filho, S. Tong, M. Ge, C. O. Della Védova, R. M. Romano, *J. Phys. Chem. A* **2013**, *117*, 9179.
- [9] Y.-L. Liu, G.-H. Hsiue, C.-W. Lan, Y.-S. Chiu, *J. Polym. Sci. Part A* **1997**, *35*, 1769.
- [10] For example, see: a) G. I. Derkatsch, *Angew. Chem. Int. Ed.* **1969**, *8*, 421–428, *Angew. Chem.* **1969**, *81*, 407–415; *Angew. Chem. Int. Ed.* **1969**, *8*, 421–428; b) C. M. Timperley, S. N. Marriott, M. J. Waters, *J. Fluorine Chem.* **2002**, *113*, *1*, 111–122.
- [11] D. Li, J. Schwabedissen, H.-G. Stämmler, N. W. Mitzel, H. Willner, X. Zeng, *Phys. Chem. Chem. Phys.* **2016**, *18*, 26245.
- [12] J. Schwabedissen, D. Q. Li, C. G. Reuter, H.-G. Stämmler, N. W. Mitzel, E. Bernhardt, X. Q. Zeng, *Z. Anorg. Allg. Chem.* **2018**, *644*, 1415.
- [13] a) D. W. H. Rankin, S. J. Cyvin, *J. Chem. Soc. Dalton Trans.* **1972**, 1277; b) P. D. Blair, *J. Mol. Struct.* **1983**, *97*, 147.
- [14] X. Q. Zeng, M. Gerken, H. Beckers, H. Willner, *Inorg. Chem.* **2010**, *49*, 3002.
- [15] X. Zeng, H. Beckers, H. Willner, R. J. F. Berger, S. A. Hayes, N. W. Mitzel, *Eur. J. Inorg. Chem.* **2011**, *2011*, 895.
- [16] a) R. A. Kendall, T. H. Dunning, R. J. Harrison, *J. Chem. Phys.* **1992**, *96*, 6796; b) T. H. Dunning, *J. Chem. Phys.* **1989**, *90*, 1007.

- [17] M. J. Frisch, G. W. Trucks, H. B. Schlegel, G. E. Scuseria, M. A. Robb, J. R. Cheeseman, G. Scalmani, V. Barone, B. Mennucci, G. A. Petersson, H. Nakatsuji, M. Caricato, X. Li, H. P. Hratchian, A. F. Izmaylov, J. Bloino, G. Zheng, J. L. Sonnenberg, M. Hada, M. Ehara, K. Toyota, R. Fukuda, J. Hasegawa, M. Ishida, T. Nakajima, Y. Honda, O. Kitao, H. Nakai, T. Vreven, J. A. Montgomery, Jr., J. E. Peralta, F. Ogliaro, M. Bearpark, J. J. Heyd, E. Brothers, K. N. Kudin, V. N. Staroverov, R. Kobayashi, J. Normand, K. Raghavachari, A. Rendell, J. C. Burant, S. S. Iyengar, J. Tomasi, M. Cossi, N. Rega, J. M. Millam, M. Klene, J. E. Knox, J. B. Cross, V. Bakken, C. Adamo, J. Jaramillo, R. Gomperts, R. E. Stratmann, O. Yazyev, A. J. Austin, R. Cammi, C. Pomelli, J. W. Ochterski, R. L. Martin, K. Morokuma, V. G. Zakrzewski, G. A. Voth, P. Salvador, J. J. Dannenberg, S. Dapprich, A. D. Daniels, Ö. Farkas, J. B. Foresman, J. V. Ortiz, J. Cioslowski, D. J. Fox, "Gaussian09.D01", 2009.
- [18] a) R. J. F. Berger, M. Hoffmann, S. A. Hayes, N. W. Mitzel, *Z. Naturforsch.* **2009**, *64b*, 1259; b) C. G. Reuter, Yu. V. Vishnevskiy, S. Blomeyer, N. W. Mitzel, *Z. Naturforsch.* **2016**, *71b*, 1.
- [19] Yu. V. Vishnevskiy, *J. Mol. Struct.* **2007**, *833*, 30.
- [20] Yu. V. Vishnevskiy, *J. Mol. Struct.* **2007**, *871*, 24.
- [21] Yu. V. Vishnevskiy, "UNEX, v. 1.6.0", <http://unexprog.org>, 2013.
- [22] a) V. A. Sipachev, *J. Mol. Struct.* **2001**, *567–568*, 67; b) V. A. Sipachev, *J. Mol. Struct.* **2004**, *693*, 235; c) V. A. Sipachev, *Struct. Chem.* **2000**, *11*, 167; d) V. A. Sipachev, *J. Mol. Struct. - THEOCHEM* **1985**, *121*, 143; e) Yu. V. Vishnevskiy, Yu. A. Zhabanov, *J. Phys. Conf. Ser.* **2015**, *633*, 012076.
- [23] CCDC 2006262 contains the supplementary crystallographic data for this paper. These data can be obtained free of charge from The Cambridge Crystallographic Data Centre via www.ccdc.cam.ac.uk/conts/retrieving.html.
- [24] O. V. Dolomanov, L. J. Bourhis, R. J. Gildea, J. A. K. Howard, H. Puschmann, *J. Appl. Crystallogr.* **2009**, *42*, 339.
- [25] a) G. M. Sheldrick, *Acta Crystallogr. Sect. C* **2015**, *71*, 3; b) G. M. Sheldrick, *Acta Crystallogr. Sect. A* **2008**, *64*, 112.
- [26] C. Möller, M. S. Plesset, *Phys. Rev.* **1934**, *46*, 618.
- [27] Y. Zhao, D. G. Truhlar, *Theor. Chem. Acc.* **2008**, *120*, 215.
- [28] a) C. Lee, W. Yang, R. G. Parr, *Phys. Rev. B* **1988**, *37*, 785; b) A. D. Becke, *Phys. Rev. A* **1988**, *38*, 3098.
- [29] J. R. Durig, J. W. Clark, *J. Chem. Phys.* **1967**, *46*, 3057.
- [30] Q. F. Liu, H. M. Li, Z. Wu, D. Q. Li, H. Beckers, G. Rauhut, X. Q. Zeng, *Chem. Asian J.* **2016**, *11*, 2953.
- [31] H. M. Li, Z. Wu, D. Q. Li, H. B. Wan, J. Xu, M. Abe, X. Q. Zeng, *Chem. Commun.* **2017**, *53*, 4783.
- [32] H. M. Li, Z. Wu, D. Q. Li, D. Bégué, C. Wentrup, X. Q. Zeng, *Chem. Eur. J.* **2016**, *22*, 7856.
- [33] X. Q. Zeng, H. Beckers, H. Willner, J. F. Stanton, *Angew. Chem. Int. Ed.* **2011**, *50*, 1720.
- [34] H. M. Li, Z. Wu, D. Q. Li, X. Q. Zeng, H. Beckers, J. S. Francisco, *J. Am. Chem. Soc.* **2015**, *137*, 10942.
- [35] X. Q. Zeng, H. Beckers, H. Willner, *Angew. Chem. Int. Ed.* **2009**, *48*, 4828.
- [36] Z. Wu, C. Song, J. Liu, B. Lu, Y. Lu, T. Trabelsi, J. S. Francisco, X. Q. Zeng, *Chem. Eur. J.* **2018**, *24*, 14627.
- [37] K. Edl, M. Krieg, D. Grote, H. F. Bettinger, *J. Am. Chem. Soc.* **2017**, *139*, 15151.
- [38] Z. Wu, H. Li, B. Zhu, X. Zeng, S. A. Hayes, N. W. Mitzel, H. Beckers, R. J. F. Berger, *Phys. Chem. Chem. Phys.* **2015**, *17*, 8784.
- [39] L. Acha, E. R. Cromie, D. W. H. Rankin, *J. Mol. Struct.* **1981**, *73*, 111.
- [40] A. Greenberg, J. F. Liebman, D. van Vechten, *Tetrahedron* **1980**, *36*, 1161.
- [41] M. C. Böhm, R. Gleiter, *Angew. Chem.* **1983**, *95*, 334.
- [42] S. Alvarez, *Dalton Trans.* **2013**, *42*, 8617.
- [43] P. M. J. Szell, A. Siiskonen, L. Catalano, G. Cavallo, G. Taerraneo, A. Priimagi, D. L. Bryce, P. Metrangolo, *New J. Chem.*, **2018**, *42*, 10467.
- [44] a) G. Cavallo, P. Metrangolo, R. Milani, T. Pilati, A. Priimagi, G. Resnati, G. Terraneo, *Chem. Rev.* **2016**, *116*, 2478; b) G. R. Desiraju, P. S. Ho, L. Kloo, A. C. Legon, R. Marquardt, P. Metrangolo, P. Politzer, G. Resnati, K. Rissanen, *Pure Appl. Chem.* **2013**, *85*, 1711.
- [45] K. Eskandari, M. Lesani, *Chem. Eur. J.* **2015**, *21*, 4739.
- [46] P. Metrangolo, J. S. Murray, T. Pilati, P. Politzer, G. Resnati, G. Terraneo, *Cryst. Growth Des.* **2011**, *11*, 4238.
- [47] C. Esterhuysen, A. Heßelmann, T. Clark, *ChemPhysChem* **2017**, *18*, 772.
- [48] a) N. Ramasubbu, R. Parthasarathy, P. Murray-Rust, *J. Am. Chem. Soc.* **1986**, *108*, 4308; b) T. Sakurai, M. Sundaralingam, G. A. Jeffrey, *Acta Crystallogr.* **1963**, *16*, 354; c) G. R. Desiraju, R. Parthasarathy, *J. Am. Chem. Soc.* **1989**, *111*, 222; d) B. K. Saha, A. Nangia, J. F. Nicoud, *Cryst. Growth Des.* **2006**, *6*, 1278.

Manuscript received: June 4, 2020

Revised manuscript received: July 7, 2020